coatings

MDPI

Article

Superhydrophobic Sands for the Preservation and Purification of Water

Yuyang Liu and Chang-Hwan Choi *

Department of Mechanical Engineering, Stevens Institute of Technology, Hoboken, NJ 07030, USA; tcliuyy@gmail.com

* Correspondence: cchoi@stevens.edu; Tel.: +1-201-216-5579

Abstract: Sand, a cheap and naturally abundant particulate material, was modified with photocatalytic and hydrophobic coatings to reduce evaporation loss and facilitate the purification of water. The first-level photocatalytic coatings (TiO_2 or ZnO nanocrystals) rendered nanoscale roughness on the surface of the sand. The additional second-level hydrophobic coating of a self-assembled monolayer of octyltrimethoxysilane (OTS) made the sand particles superhydrophobic because of the nanoscale roughness imposed by the nanocrystals. The superhydrophobic sand particles, floating on the free surface of water due to their superhydrophobicity, significantly reduced the evaporation loss of water by 60%–90% in comparison to an uncovered water surface. When the outer hydrophobic coatings are weathered or disengaged, the inner photocatalytic coatings become exposed to water. Then, the sand particles act as photocatalysts to degrade the contaminants in water under solar radiation.

Keywords: sand; photocatalysts; superhydrophobic; water; evaporation; purification

Citation: Liu, Y.; Choi, C.-H. Superhydrophobic Sands for the Preservation and Purification of Water. *Coatings* **2021**, *11*, 151. https://doi.org/10.3390/coatings11020151

Received: 13 November 2020
Accepted: 26 January 2021
Published: 29 January 2021

1. Introduction

Water is the most important resource on earth and it has become a more valuable commodity as concerns increase about its scarcity and sustainability [1]. The run-off water stored in ponds, ditches, and dams is extensively used as a water supply for industrial, agricultural, and even domestic applications. In fact, as much as 40%, of water stored in a farm dam can be lost through evaporation, depending on the condition of the dam and the local weather [2]. The evaporation loss can be reduced through both physical and chemical strategies. Furthermore, the evaporation loss can be significantly decreased through specialized dam design, including reducing the surface area to volume ratio (e.g., using deeper and narrower dams) and planting windbreaks to provide shade and diminish wind turbulence. However, the construction of water dams with such structures is challenging and a serious financial burden for many developing countries and districts. Covering the surface of the water body with waterproof plastic films is an alternative way to effectively reduce evaporation loss [3]. When the plastic floating barrier covers 80% of the water surface, it has the potential to reduce evaporation by an average of about 70% annually [4]. The main advantage of using plastic floating barriers on water bodies is that they provide long-term protection from evaporation loss; however, they are not cost-effective. They can also block sunlight, which can seriously facilitate the growth of aquatic plants and make the water dirty. Furthermore, spreading plastic barriers or films over a large water body is dangerous and needs to be done by trained professionals. For example, floating solar panels have been used recently to cover large water bodies to suppress evaporation and generate power [5], which involves expensive equipment and a complicated assembly process.

The use of chemical barriers can mitigate such issues [6]. It has long been known that the evaporation rate of water can be reduced by applying oil to its surface [7,8]. For example, oil has been used upon inland rivers and lakes to retard evaporation and

thereby reduce the formation of fog [9]. Among various types of oils, long-chain alcohol or acid is very attractive and efficient for this purpose. When spread on water, the monolayer molecules are oriented with the hydrophilic end (–OH groups) buried in the water and the hydrophobic end (the hydrocarbon chain) facing out into the air, forming a thin monolayer barrier on the water surface. It has been reported that the monolayer barriers' resistance to evaporation rises with the length of the hydrocarbon chain [10,11]. The efficiency of these compounds as evaporation retardants, however, is increasingly hampered by progressively higher melting points, which reduce their ability to spread on the water surface [11,12]. Some new compounds with low melting points have been developed [13]. These chemical barriers mainly use long-chain alcohols such as cetyl-, stearyl-, and aliphatic alcohols to spread a film over the water surface [14,15]. However, so far, they have had limited application in field trials. It has been reported that this approach can reduce evaporation loss by 15%–30% [7–15], which is less efficient than the physical covering method. Depending on the weather conditions around the water body, re-treatment is often required every two to four days, and thus only effective for the short-term protection of the water body from evaporation loss; however, it is still the most affordable option. The chemical barriers can be applied seasonally when they are most needed. Most chemical barriers do not block too much sunlight and are environmentally benign and eco-friendly.

In this study, we report a new strategy that combines the merits of both the physical and chemical approaches. The use of the easily obtainable and cheap particulate material, sand, as a physical barrier, can significantly reduce the evaporation loss. In order for them to work as effective floating barriers, the surface of sand particles is modified to be superhydrophobic by dual coatings. The first coating is created by growing photocatalytic nanoparticulates such as ZnO and TiO_2, and self-assembled monolayer hydrophobic coatings are applied as the second coating for chemical barriers. The photocatalytic nanoparticles enhance the non-wettability of the sand because of their structural roughness [16–18], and they can also purify the water via the photocatalytic process that occurs under the irradiation of sunlight [19–23]. In this way, our approach provides a new, cheap, and eco-friendly method to reduce the evaporation loss of dams, ponds, ditches, and lakes with the additional benefit of the purification of the water.

The treatment of sand to produce hydrophobic properties for different applications has been reported by several researchers [24–28]. Gao et al. [24] coated sand with graphite oxide materials for water purification applications. Hoffman et al. [25] studied the application of hydrophobic sand for urine collection. They found a minimal risk of internal contamination in a study involving a rat by the hydrophobic sand, and no interference of the sand with several common metals. Chen et al. [26,27] studied treated sand for water reservations. They found that superhydrophobic sand has a great potential for water-holding capacity in such a way that a superhydrophobic sand layer with a thickness of 2 cm could sustain a water column with a height of 35 cm. The superhydrophobic sand also demonstrated a great anti-flow-dragging effect during water transportation, whereby a water droplet could smoothly and quickly roll down a simulated sand channel. Liu et al. [28] fabricated superhydrophobic sand by structuring polydopamine and TiO_2 coatings followed by a hydrophobic modification with perfluorodecyltrichlorosilane (FDTS). The superhydrophobic sand also showed good water-holding capacity as well as oil/water separation and anti-icing properties. However, so far, no attempts have been made to design and apply superhydrophobic sand for the dual functions of water reservation and purification. In this study, the dual functions of superhydrophobic sand are realized by the coating of functional nanomaterials, such as ZnO and TiO_2, on sand particles before hydrophobization. The superhydrophobicity, the gateable property for water penetration, the reduction in evaporation loss, and the photocatalytic purification efficacy of the dual-coated superhydrophobic sand for water are experimentally investigated in this study.

2. Materials and Methods

2.1. Preparation of Sand

Sand grains were collected from a local desert. The particle size of the sand varied from 0.1 to 2.2 mm. The apparent density of the sand was 1.722 g/cm^3, measured by packing raw sand into a 100 mL precision measuring cylinder (BLAUBRAND® Graduated Cylinder, Cole-Parmer, IL, USA). Apparent density is the average value of two measurements. The raw sand particles were first rinsed with tap water 2–3 times, then rinsed with ethanol (purity 99.5%) to remove impurities, and dried at 120 °C for 30 min in a preheated oven. The dried sand particles were then cooled down to room temperature and screened with a stainless-steel mesh sieve (0.600 mm sieve opening No. 30). The sand particles were then coated with TiO_2 or ZnO nanocrystals through a sol-gel process or using the hydrothermal method, which are both described below.

2.2. TiO_2 Sol-Gel Coating

The detail of the sol-gel process for TiO_2 coating is as follows: First, 100 g of sand was added to 200 mL of an acid solution containing 4% acetic acid under mechanical stirring. The mixture was then heated to 90 °C with a hot plate. Eight mL of titanium isopropoxide was slowly added to the mixture under mechanical stirring. The mixture was kept at 90 °C for 2 h and then cooled down to room temperature. Sand was recovered through filtration and washed with deionized water multiple times. The treated sand was dried at 100 °C for 20 min in a preheated oven.

2.3. ZnO Hydrothermal Coating

The hydrothermal method for ZnO coating is as follows: First, 6.6 g of zinc acetate dihydrate was dissolved in 200 mL of deionized water. Then, 100 g of sand was added to the solution under mechanical stirring. Ten mL of ammonia (25 wt.%) was added to the mixture under stirring. The mixture was heated to 95 °C with a hot plate and kept at 95 °C for 1 h. Then, the mixture was cooled down to room temperature. The sand was recovered by filtration and washed with water multiple times. The treated sand was dried at 100 °C for 20 min in a preheated oven.

2.4. Hydrophobic Coating

The sand, functionalized with TiO_2 or ZnO, was further treated to produce hydrophobicity using the self-assembled monolayer (SAM) coating of octyltrimethoxysilane (OTS). The SAM solution was prepared by mixing 2 mL of OTS with 500 mL of ethanol (7.8 mM) at room temperature and stirred for 20 min in a glovebox with a N_2 atmosphere before use. The dried sand was transferred to and soaked in the solution for 2 h, with the solution constantly and gently being stirred by a mechanical stirrer. The sand was then recovered with a centrifugal separator, washed with ethanol multiple times, and subsequently washed with deionized water and dried at 120 °C in a preheated oven for 30 min. All the chemical reagents used in this study were purchased from Sigma-Aldrich (St. Louis, MO, USA) and used as received without further purification.

3. Results and Discussion

3.1. Fourier-Transform Infrared Spectroscopy (FTIR) Analysis

The coatings of TiO_2 or ZnO on silicon oxide surfaces, such as glass and sand, were used for various applications [28–30]. The self-assembled monolayer coating of OTS on oxide surfaces was also widely used for hydrophobization [31]. We confirmed the chemical compositions of the coatings by FTIR analysis. The FTIR was collected with the Smart iTR™ Attenuated Total Reflectance (ATR) sampling accessory attached to the Nexus-470 FTIR spectrometer (Thermo Scientific, Waltham, MA, USA). A ~0.09 g sample of the prepared superhydrophobic sand was placed on the sample holder, the pressure tower was carefully tightened to hold the samples, and then the samples were scanned from 4000 to 600 cm^{-1}. For example, Figure 1a–c show the FTIR of the pristine sand and

the TiO_2-coated sand before and after the OTS coating, respectively. The peaks around 2800–3000, 1430, 1100, and 910 cm^{-1} represent the absorptions for C–H, Ti–O–Ti, Si–O–Si, and Ti–O–Si bonds, respectively, confirming the successive coatings of the TiO_2 and OTS on the sand particles. Such coatings generally form stable, covalent bonds with high energy that are durable in varying conditions, such as temperature, solvent, and humidity [28–31].

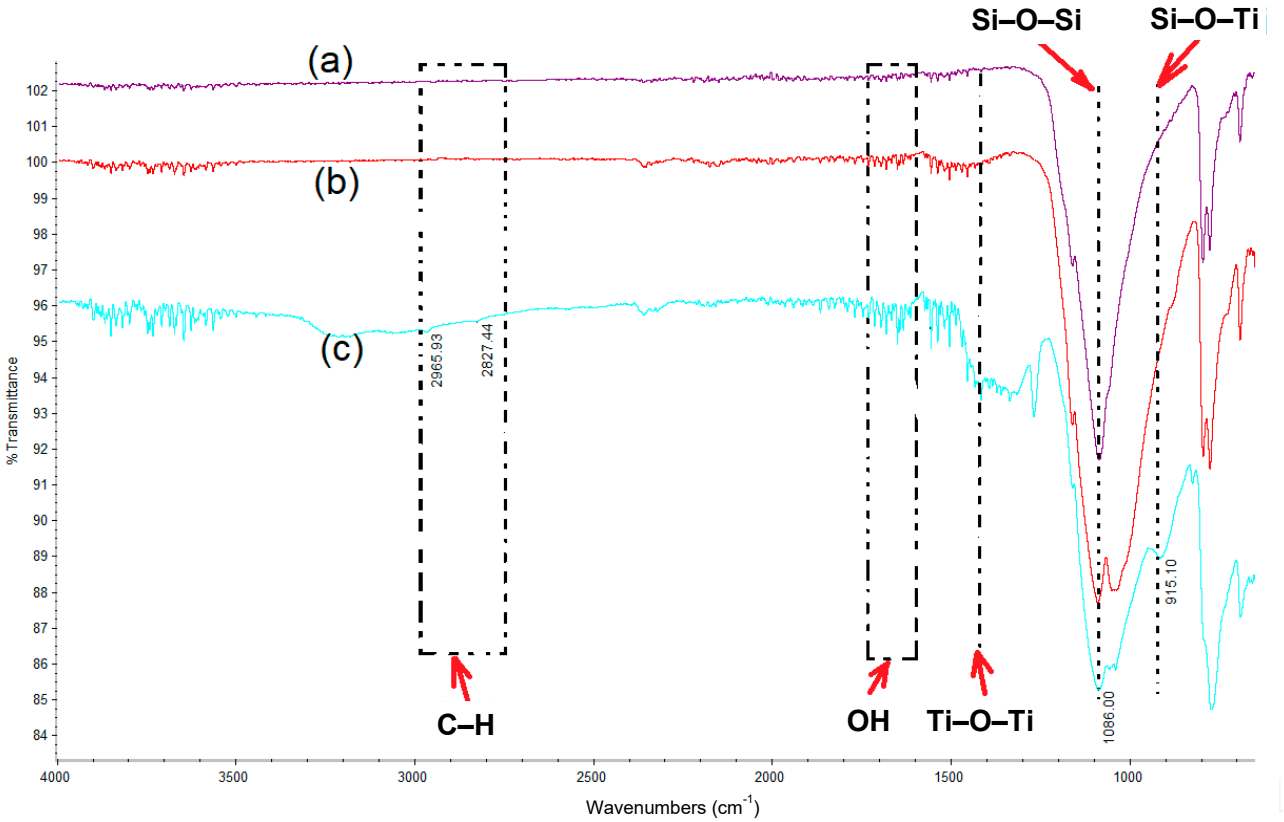

Figure 1. FTIR spectroscopy of the sands. (**a**) Pristine sand. (**b**) TiO_2-coated sand. (**c**) TiO_2-coated sand with the further coating of OTS.

3.2. Surface Morphology

Figure 2 shows the surface morphologies of the pristine sand, the TiO_2-coated sand, and the ZnO-coated sand, respectively, measured by scanning electron microscopy (SEM, Auriga Small Dual-Beam FIB-SEM, Zeiss, Oberkochen, Germany). Compared to the pristine sand, the sand particles functionalized with the nanomaterials exhibited nanoscale granules (around 50–100 nm in size) whose shapes and grains were irregular. The OTS hydrophobic coating did not alter the morphology of the surfaces due to the nature of the self-assembled monolayer coating with a uniform film thickness of ~2 nm [31].

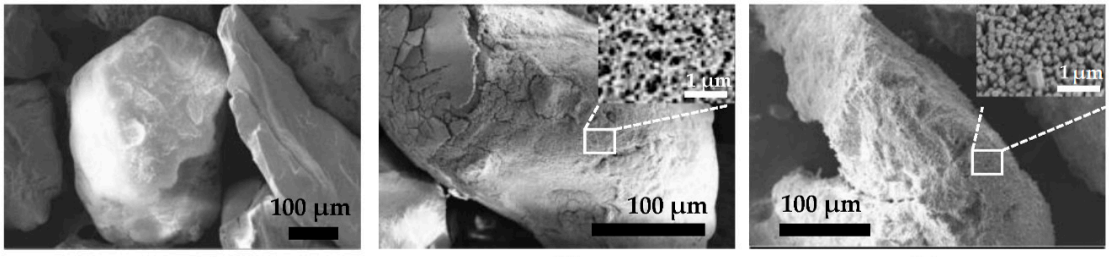

(a) (b) (c)

Figure 2. SEM images of sand. (**a**) Pristine sand. (**b**) TiO_2-coated sand. (**c**) ZnO-coated sand.

3.3. Superhydrophobicity

Figure 3 shows the wettability of the further hydrophobized sand. For example, Figure 3a shows the optical image of a water droplet (50 μL) sitting on the hydrophobized TiO_2-coated sand. A thin layer of sand was prepared on the top side of a piece of Scotch® double-sided tape, while the bottom side was attached to the sample stage of a customized contact angle meter equipped with a digital zoom microscope (SUNS004001-P, Sunnywoo, Shenzhen, China). The measured contact angle was ~150°. The advancing and receding contact angles were also measured for the contact angle hysteresis (i.e., the difference between the advancing and receding contact angles), while the sample stage was gradually tiled. As shown in Figure 3b, the droplet started to slide on the surface at the inclination of ~15°, where the advancing and receding contact angles were ~160° and ~145°, respectively, resulting in a contact angle hysteresis of ~15°. The high apparent contact angle coupled with the low sliding angle and contact angle hysteresis indicates that the hydrophobized sand supports the Cassie–Baxter superhydrophobicity (i.e., partial wetting, with air retained between the hydrophobized sand particulates). Figure 3c shows water droplets (colored with blue ink for clearer visualization) of varying sizes (50–200 μL) sitting on the superhydrophobic sand, which was randomly placed on a glass surface. The droplets did not wet the superhydrophobic sand but formed 'drying beads' on it. Figure 3d further shows the water droplet placement on the superhydrophobic sand, which was spread and floating on the free surface of a bulk water body. Instead of sinking down into the water, the superhydrophobic sand formed a thin layer on the free surface and floated because of the surface tension effects, despite having a higher density than water. The floating sand layer showed good stability on the water surface. As shown in Figure 3d, even when placing a relatively large water droplet (0.2 mL) on the floating sand layer, the superhydrophobic sand layer held the droplet firmly on its surface.

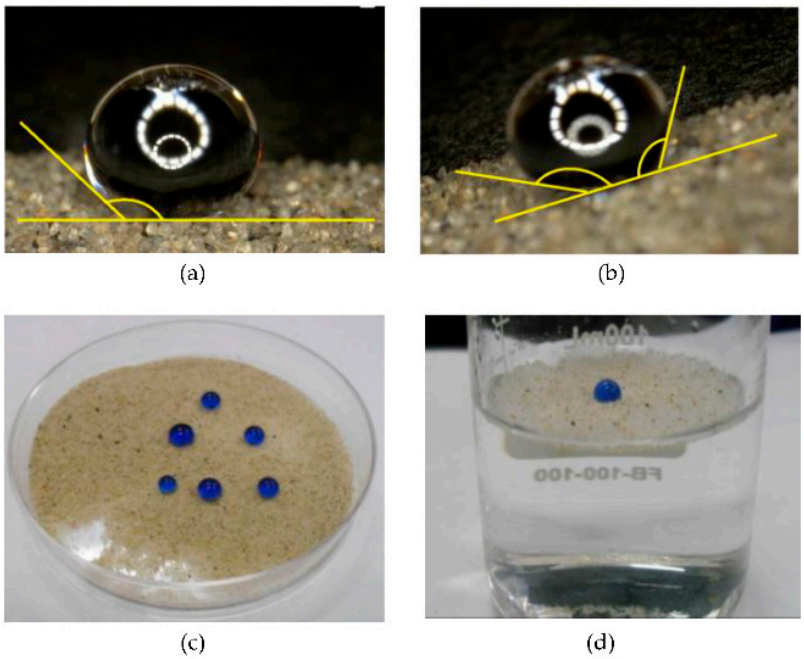

Figure 3. Superhydrophobicity of the hydrophobized sand coated with the functional nanomaterials TiO_2 or ZnO. (**a**) Optical graph of a water droplet sitting on a horizontally leveled surface of the hydrophobized sand. (**b**) Optical graph of a water droplet sliding on a tiled surface of the hydrophobized sand. (**c**) Optical graph of water droplets of varying sizes (colored with blue ink for clearer visualization) sitting on the superhydrophobic sand spread on a glass surface. (**d**) Optical graph of a water droplet of ~0.2 mL (colored with blue ink for clearer visualization) sitting on the superhydrophobic sand spread and floating on the free surface of water.

3.4. Gateable Property for Water Penetration

In addition, the floating superhydrophobic sand freely moved under relatively high forces such as pressurized flows. Figure 4 shows such an experiment where a pressurized water jet flow (colored with blue ink for visualization purposes) was applied to the superhydrophobic sand layer floating on the free surface of water. It shows that the pressurized water flow penetrated the floating superhydrophobic sand layer and merged with the water body underneath the layer. When the jet flow was halted, the thin layer of superhydrophobic sand reformed and immediately uniformly covered the free surface once again. Such a gateable property for water penetration is one of the advantages of using the superhydrophobic sand as a barrier for evaporation loss compared to other types of barriers, such as plastic barriers or chemical barriers. For example, when it rains, the high-speed rain droplets are able to effectively penetrate the floating superhydrophobic sand layer and merge with the water body. Thus, they are stored in the reservoir, instead of being wasted.

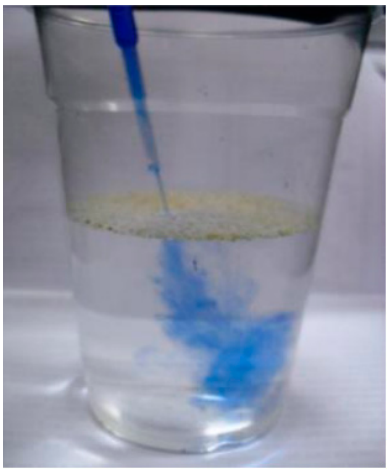

Figure 4. Water-penetrating or gateable property of the superhydrophobic sand floating on the free surface of water.

3.5. Reduction in Evaporation Loss

The reduction in the evaporation loss by the superhydrophobic sand was evaluated by measuring the mass change of water stored in open dishes (9 cm in diameter, ~64 cm^2 for the open surface area). Two dishes were prepared: one with a fully open, free surface that was used as a control, and another for the floating superhydrophobic sand, to compare with the control. In addition, 50 g of deionized water was deposited into the dishes. Then, in the second dish only, 1.0 g of superhydrophobic sand was spread over the water surface to form a thin (~1 mm) sand layer. Next, both dishes were left to evaporate at 25 °C and 55% RH. The mass of water in both dishes was measured hourly with a precise balance. Five parallel experiments were conducted, and their average and standard deviation values were analyzed. Two different cases were tested and analyzed, one with no flow, and the other with wind. In the case with wind, the evaporation experiment was carried out in a fume hood with a wind speed at 3.5 m/s at 25 °C and 55% RH.

Figure 5a shows the result of the evaporative mass loss of the water body tested in a static (no flow) condition up to 10 h. In the case of no barrier, the average evaporation rate of water over the 64 cm^2 open surface was measured to be 1.035 mL/h. After evaporation for 10 h, ~11 g of water had evaporated out. In contrast, when the free surface of water was protected with the layer of superhydrophobic sand, the evaporation rate was significantly reduced to 0.1 mL/h (around ten times lower than that of the unprotected water) and only ~1 g of water was lost from evaporation. As a result, the floating superhydrophobic sand layer effectively reduced the evaporation loss by more than 90%. There was no significant difference between the TiO_2-coated and ZnO-coated sands.

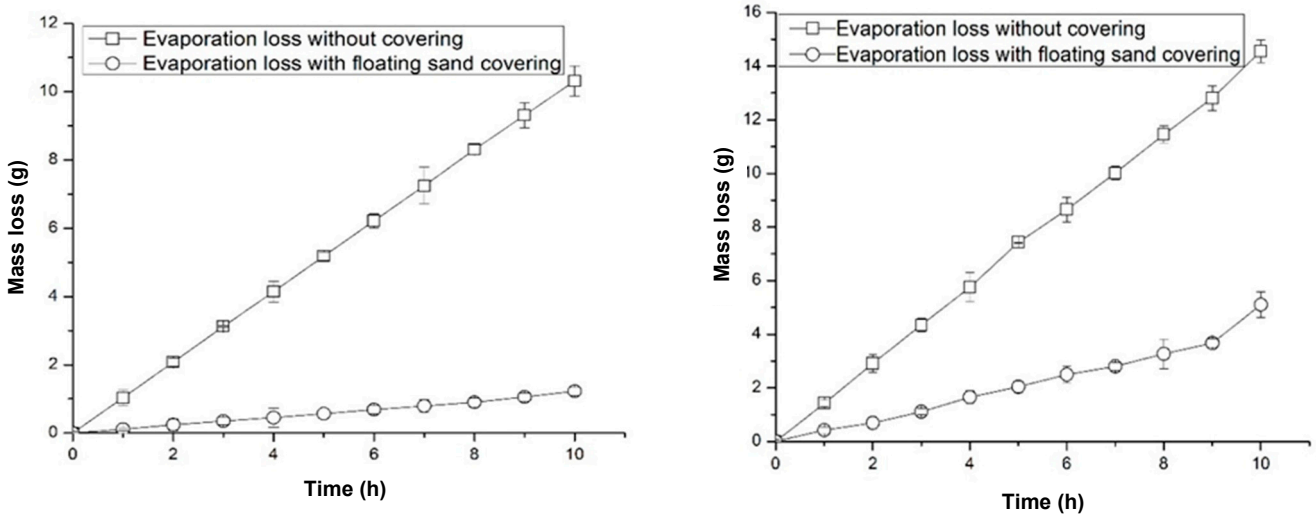

Figure 5. Evaporation loss of water. (**a**) Under no wind. (**b**) Under wind (3.5 m/s).

Figure 5b shows the results obtained in the dynamic (with wind) condition. In the case of the uncovered water, the average evaporation rate was measured to be ~1.5 mL/h, which is ~50% higher than that measured in the static (no wind) condition. In the case of the water covered with the superhydrophobic sand layer, the evaporation rate was ~0.5 ml/h, about five times higher than the rate measured in the static condition. However, compared to the uncovered water, the superhydrophobic sand barrier still significantly reduced the evaporation rate (by up to ~66%), even in the condition with relatively high-speed wind (3.5 m/s). After the evaporation for 10 h, the evaporation loss of water was ~15 g in the case of the uncovered water, whereas it was only ~5 g in the case of the water protected by the barrier layer of superhydrophobic sand.

3.6. Photocatalytic Water Purification

Extensive research has shown that under sunlight (ultraviolet (UV) irradiation), photocatalytic nanoparticles or nanostructures such as TiO_2 and ZnO can break down a wide variety of organic materials, organic acids, estrogens, pesticides, dyes, crude oil, microbes (including viruses and chlorine resistant organisms), and inorganic molecules such as nitrous oxides (NO_x) [32]. Combined with precipitation or filtration methods, these photocatalytic nanomaterials can also remove toxic metals such as mercury [33]. Thus, the sand coated with TiO_2 or ZnO nanocrystals can be directly used as a photocatalyst for water purification [34,35]. With the additional hydrophobic coating, the superhydrophobic sand coated with TiO_2 or ZnO nanocrystals first works as a floating barrier for the reduction in evaporation loss. Then, when it loses its hydrophobicity, as a result of weathering effects such as UV radiation [36], it will precipitate onto the bottom of the water body and continue to act as a photocatalyst for water purification. In laboratory conditions, the superhydrophobic sand can float on the free surface of water for several months. However, in outdoor conditions, the floating sand will gradually lose its hydrophobicity (e.g., from the degradation, destruction, or fouling of the hydrophobic coatings) and precipitate onto the bottom of the water body in less time.

The photocatalytic efficacy of the functionalized sand (without hydrophoziation) was evaluated according to a published method [29] and compared with the pristine sand. Ten grams of sand were transferred into 1000 mL of wastewater containing 0.2 g of azo-dye (Cibacron Blue F-R). The beakers containing the wastewater with the different types of sands as well as the beaker with no sand (used as the control) were irradiated with a UV light (365 nm, TLD 18W/08, Philips, Amsterdam, The Netherlands) at the intensity of 1.5 mW·cm^2. The concentration of the dye in each water sample was measured hourly

according to the change of UV-Vis absorption intensity at 610 nm (UV-Vis spectrometer Lambda 18, Perkin Elmer, Waltham, MA, USA) [29]. Figure 6 shows the results of the photocatalytic efficacy of the sands for the degradation of azo-dye in water. In the wastewater with no sand (used as the control), the concentration of azo-dye did not change significantly during the UV-irradiation for 3.5 h. In the wastewater with the pristine sand, a slight decrease in the concentration was shown in the beginning (from 200 to 170 mg/L in 0.5 h). However, no significant decrease was measured afterward. The initial effect of the decrease was attributed to the physical adsorption of contaminants (dye) onto the sand particles. In the wastewater with the sand functionalized with TiO_2 and ZnO, the concentration of azo-dye in both cases was significantly reduced after the UV irradiation (more than 50% within an hour). The result indicates that the photocatalytic effects of the functionalized sand were highly significant to break down the azo-dye molecules.

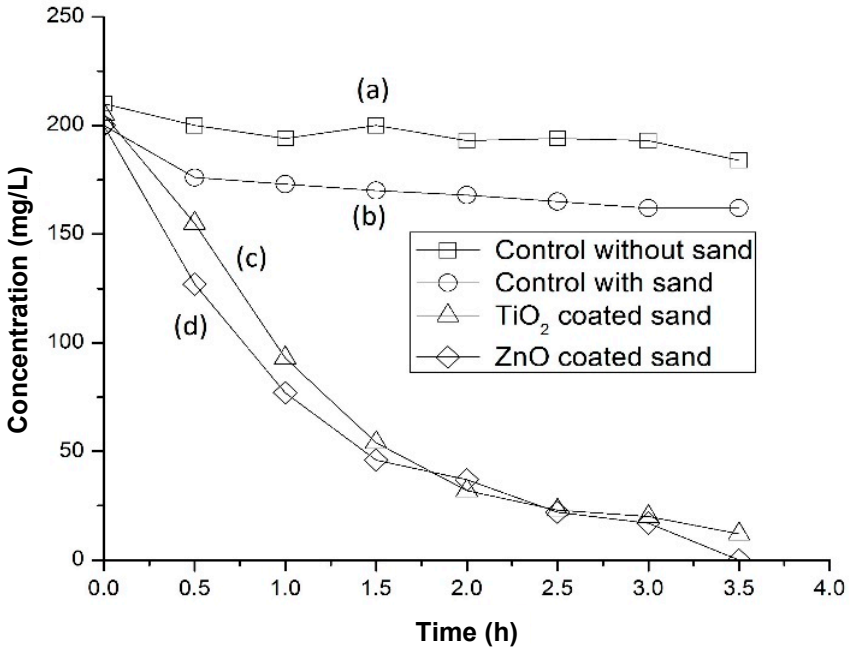

Figure 6. Photocatalytic efficacy of the functionalized sands for the degradation of azo-dye in water. (**a**) Wastewater without sand. (**b**) Wastewater with 10 g of pristine sands. (**c**) Wastewater with 10 g of TiO_2-coated sands. (**d**) Wastewater with 10 g of ZnO-coated sands.

4. Conclusions

Sand, a naturally abundant raw material, was coated with photocatalytic nanoparticles and a self-assembled monolayer hydrophobic coating to reduce evaporation loss from and facilitate the UV-based purification of a body of water. Floating on the free surface of a water body, the superhydrophobic sand layer acts as both a physical and chemical barrier to prevent water molecules from evaporating. Although the individual sand particles are very small (in the order of 0.1–1 mm), they form a large film and physically protect the water surface when they are spread on the water. At the same time, the interface between the superhydrophobic sand and the water provides a chemical energy barrier for water molecules to overcome evaporation. As a result, the floating superhydrophobic sand layer reduces the evaporation loss of a water body significantly. When the superhydrophobic sand loses its hydrophobicity (e.g., the outer layer of hydrophobic coating), the photocatalytic layer becomes fully exposed to the water body and enables the purification of water. After its use, the sand material can be returned to nature or recycled with proper and necessary treatment of the nanoparticles to avoid negative impacts to humans and natural environments [37–39]. Superhydrophobic sand can thus provide a new, cheap, and effective method for the preservation and purification of water in real applications.

Author Contributions: Conceptualization, Y.L. and C.-H.C.; methodology, Y.L.; software, Y.L.; validation, Y.L. and C.-H.C.; formal analysis, Y.L.; investigation, Y.L.; resources, C.-H.C.; data curation, Y.L. and C.-H.C.; writing—original draft preparation, Y.L.; writing—review and editing, C.-H.C.; visualization, Y.L.; supervision, C.-H.C.; project administration, C.-H.C.; funding acquisition, C.-H.C. Both authors have read and agreed to the published version of the manuscript.

Funding: This research received no external funding.

Institutional Review Board Statement: Not applicable.

Informed Consent Statement: Not applicable.

Data Availability Statement: The data presented in this study are available in article.

Conflicts of Interest: The authors declare no conflict of interest.

References

1. Gleick, P.H. *The World's Water*; Island Press: Washington, DC, USA, 2011; Volume 3.
2. Craig, I.; Green, A.; Scobie, M.; Schmidt, E. *Controlling Evaporation Loss from Water Storages*; National Center for Engineering in Agriculture Publication: Toowoomba, Australia, 2005.
3. Assouline, S.; Narkis, K.; Or, D. Evaporation suppression from water reservoirs: Efficiency considerations of partial covers. *Water Resour. Res.* **2011**, *47*, W07506. [CrossRef]
4. Yao, X.; Zhang, H.; Lemckert, C.; Brook, A.; Schouten, P. *Evaporation Reduction by Suspended and Floating Covers: Over-View, Modelling and Efficiency*; Technical Report No. 28; Urban Water Security Research Alliance: Brisbane, Australia, 2011.
5. Mittal, D.; Saxena, B.K.; Rao, K.V.S. Potential of floating photovoltaic system for energy generation and reduction of water evaporation at four different lakes in Rajastha. In Proceedings of the 2017 International Conference On Smart Technologies For Smart Nation (SmartTechCon), Bangalore, India, 17–19 August 2017; pp. 238–243.
6. La Mer, V.K. *Retardation of Evaporation by Monolayers*; Elsevier Inc.: New York, NY, USA, 1962.
7. Roberts, W.J. Evaporation suppression from water surfaces. *Trans. Am. Geophys. Union* **1957**, *38*, 740–744. [CrossRef]
8. Roberts, W.J. Reducing lake evaporation in the midwest. *J. Geophys. Res.* **2012**, *64*, 1605–1610. [CrossRef]
9. Frenkiel, J. *Evaporation Reduction: Physical and Chemical Principles and Review of Experiments*; UNESCO: Paris, France, 1965.
10. Barnes, G. The potential for monolayers to reduce the evaporation of water from large water storages. *Agric. Water Manag.* **2008**, *95*, 339–353. [CrossRef]
11. Henry, D.J.; Dewan, V.I.; Prime, E.L.; Qiao, G.G.; Solomon, D.H.; Yarovsky, I. Monolayer structure and evaporation resistance: A molecular dynamics study of octadecanol on water. *J. Phys. Chem. B* **2010**, *114*, 3869–3878. [CrossRef] [PubMed]
12. Mansfield, W.W. Influence of monolayers on the natural rate of evaporation of water. *Nature* **1955**, *175*, 247–249. [CrossRef]
13. Aminzadeh, M. Evaporation suppression and energy balance of water reservoirs covered with self-assembling floating elements. *Hydrol. Earth Syst. Sci.* **2018**, *22*, 4015–4032. [CrossRef]
14. Simko, A.J.; Dressler, R.G. Investigation of C_{20} to C_{25} fatty alcohols and blends as water evaporation retardants. *Ind. Eng. Chem. Prod. Res. Dev.* **1969**, *8*, 446–450. [CrossRef]
15. Fukuda, K.; Kato, T.; Machida, S.; Shimizu, Y. Binary mixed monolayers of polyvinyl stearate and simple long-chain compounds at the air/water interface. *J. Colloid Interface Sci.* **1979**, *68*, 82–95. [CrossRef]
16. Wenzel, R.N. Resistance of solid surfaces to wetting by water. *Ind. Eng. Chem.* **1936**, *28*, 988–994. [CrossRef]
17. Cassie, A.B.D.; Baxter, S. Wettability of porous surfaces. *Trans. Faraday Soc.* **1944**, *40*, 546–551. [CrossRef]
18. Lafuma, A.; Quéré, D. Superhydrophobic states. *Nat. Mater.* **2003**, *2*, 457–460. [CrossRef] [PubMed]
19. Sun, R.-D.; Nakajima, A.; Fujishima, A.; Watanabe, T.; Hashimoto, K. Photoinduced surface wettability conversion of ZnO and TiO_2 thin films. *J. Phys. Chem. B* **2001**, *105*, 1984–1990. [CrossRef]
20. Fujishima, A.; Zhang, X.; Tryk, D.A. TiO_2 photocatalysis and related surface phenomena. *Surf. Sci. Rep.* **2008**, *63*, 515–582. [CrossRef]
21. Wang, R.; Hashimoto, K.; Fujishima, A.; Chikuni, M.; Kojima, E.; Kitamura, A.; Shimohigoshi, M.; Watanabe, T. Light-induced amphiphilic surfaces. *Nature* **1997**, *388*, 431–432. [CrossRef]
22. Sakai, N.; Fujishima, A.; Watanabe, T.; Hashimoto, K. Quantitative evaluation of the photoinduced hydrophilic conversion properties of TiO_2 thin film surfaces by the reciprocal of contact angle. *J. Phys. Chem. B* **2003**, *107*, 1028–1053. [CrossRef]
23. Machida, M.; Norimoto, K.; Watanabe, T.; Hashimoto, K.; Fujishima, A. The effect of SiO_2 addition in super-hydrophilic property of TiO_2 photocatalyst. *J. Mater. Sci.* **1999**, *34*, 2569–2574. [CrossRef]
24. Gao, W.; Majumder, M.; Alemany, L.B.; Narayanan, T.N.; Ibarra, M.A.; Pradhan, B.K.; Ajayan, P.M. Engineered graphite oxide materials for application in water purification. *ACS Appl. Mater. Interfaces* **2011**, *3*, 1821–1826. [CrossRef]
25. Hoffman, J.F.; Vergara, V.B.; Mog, S.R.; Kalinich, J.F. Hydrophobic sand is a non-toxic method of urine collection, appropriate for urinary metal analysis in the rat. *Toxics* **2017**, *5*, 25. [CrossRef]
26. Chen, L.; Si, Y.; Guo, Z.; Liu, W. Superhydrophobic sand: A hope for desert water storage and transportation projects. *J. Mater. Chem. A* **2017**, *5*, 6416–6423. [CrossRef]

27. Chen, L.; Wu, Y.; Guo, Z. Superhydrophobic sand grains structured with aligned $Cu(OH)_2$ nano-needles for efficient oily water treatment. *Mater. Des.* **2017**, *135*, 377–384. [CrossRef]
28. Liu, S.; Cai, T.; Shen, X.; Huang, E.; Wang, Z.; Sun, Q. Superhydrophobic sand with multifunctionalities by TiO_2-incorporated mussel-inspired polydopamine. *Ceram. Int.* **2019**, *45*, 21263–21269. [CrossRef]
29. Qi, K.; Chen, X.; Liu, Y.; Xin, J.H.; Mak, C.L.; Daoud, W.A. Facile preparation of anatase/SiO_2 spherical nanocomposites and their application in self-cleaning textiles. *J. Mater. Chem.* **2007**, *17*, 3504–3508. [CrossRef]
30. Ebert, D.; Bhushan, B. Transparent, superhydrophobic, and wear-resistant coatings on glass and polymer substrates using SiO_2, ZnO, and ITO nanoparticles. *Langmuir* **2012**, *28*, 11391–11399. [CrossRef]
31. Srinivasan, U.; Houston, M.; Howe, R.T.; Maboudian, R. Alkyltrichlorosilane-based self-assembled monolayer films for stiction reduction in silicon micromachines. *J. Microelectromechanical Syst.* **1998**, *7*, 252–260. [CrossRef]
32. Mattle, M.J.; Thampi, K.R. Photocatalytic degradation of Remazol Brilliant Blue® by sol–gel derived carbon-doped TiO_2. *Appl. Catal. B Environ.* **2013**, *140–141*, 348–355. [CrossRef]
33. Tsai, C.-Y.; Kuo, T.-H.; Hsi, H.-C. Fabrication of Al-doped TiO_2 visible-light photocatalyst for low-concentration mercury removal. *Int. J. Photoenergy* **2012**, *2012*, 1–8. [CrossRef]
34. Dimapilis, E.A.; Hsu, C.S.; Mendoza, R.M.; Lu, M.C. Zinc oxide nanoparticles for water disinfection. *Sustain. Environ. Res.* **2018**, *28*, 47–56.
35. Stylidi, M.; Kondarides, D.I.; Verykios, X.E. Mechanistic and kinetic study of solar-light induced photocatalytic degradation of Acid Orange 7 in aqueous TiO_2 suspensions. *Int. J. Photoenergy* **2003**, *5*, 59–67. [CrossRef]
36. Lu, Y.; Xiao, S.; Gao, R.; Li, J.; Sun, Q. Improved weathering performance and wettability of wood protected by CeO_2 coating deposited onto the surface. *Holzforschung* **2014**, *68*, 345–351. [CrossRef]
37. Buzea, C.; Pacheco, I.I.; Robbie, K. Nanomaterials and nanoparticles: Sources and toxicity. *Biointerphases* **2007**, *2*, MR17–MR71. [CrossRef] [PubMed]
38. Gupta, R.; Xie, H. Nanoparticles in daily life: Applications, toxicity and regulations. *J. Environ. Pathol. Toxicol. Oncol.* **2018**, *37*, 209–230. [CrossRef] [PubMed]
39. Sengul, A.B.; Asmatulu, E. Toxicity of metal and metal oxide nanoparticles: A review. *Environ. Chem. Lett.* **2020**, *18*, 1659–1683. [CrossRef]